


Research Article

Controlling Transformer Magnetizing Offset Current in Isolated Phase-Shift Full-Bridge Converters Using a Luenberger Observer

Angelika Neumann ¹, Sönke Meynen,¹ Ahmad Rahmoun,² Daniel Ziegler,² and Thomas Kirchartz³

¹Karlsruhe University of Applied Sciences, Karlsruhe, Germany

²Ads-tec Energy GmbH, Nürtingen, Germany

³Forschungszentrum Jülich, Jülich, Germany

Correspondence should be addressed to Angelika Neumann; angelika.neumann@h-ka.de

Received 21 June 2022; Revised 28 July 2022; Accepted 8 August 2022; Published 26 September 2022

Academic Editor: mahdiyeh eslami

Copyright © 2022 Angelika Neumann et al. This is an open access article distributed under the Creative Commons Attribution License, which permits unrestricted use, distribution, and reproduction in any medium, provided the original work is properly cited.

This paper proposes a flexible digital control scheme for isolated phase-shift full-bridge (PSFB) converters. The required transformer suffers from inevitable imbalance of magnetic flux resulting in an increased magnetizing DC-offset current that threatens system reliability due to saturation effects. The paper addresses two major issues of the occurrence of a magnetizing DC-offset current. First, caused by the change of duty cycle due to output power regulation and second caused by initial manufacturer tolerances of devices. In contrast to common methods the novel control scheme uses a Luenberger observer to estimate the magnetizing current requiring only simple measurement of transformer voltages without additional and lossy auxiliary networks. The observer model, in combination with a PI-controller, directly interventions the duty cycle and removes any DC-offset current resulting from both issues. A detailed deviation of the state-space model of the transformer and a subsequently design of the observer are presented. Simulation and experimental results on a PSFB prototype verify the principal functionality of the proposed control scheme to prevent transformer saturation.

1. Introduction

Regarding the worldwide increasing climate problematic the portion of clean and renewable energy generation has increased over three-fold since the last ten years [1]. Unfortunately, renewable energies like photovoltaic (PV) or wind power reduce the reliability of power generation with its dependency on weather conditions [2, 3]. To utilize the maximum capacity of fluctuating renewable energies different storage technologies have been developed. Although lithium-ion battery systems are not the only solution to store energy, this technology has prevailed in various mobile DC-DC applications and also becomes more and more important for the high and medium power DC-DC charging sector. Typically, high power DC-DC systems use a liquid cooling system due to large heat development while charging batteries, but especially non-industrial DC-DC applications

with medium power have to manage cooling without liquid cooling system and therefore a high efficiency is very important [4].

The high efficiency and power density of an isolated phase-shift full-bridge (PSFB) converter in Figure 1 make this topology very attractive for DC-DC medium and high power applications such as DC-storage battery systems for PV or battery chargers for electric vehicles [5–7]. Its phase-shift control scheme allows for zero-voltage-switching (ZVS) operation with negligible switching losses and reaches higher efficiency compared to conventional hard-switched topologies [8].

Two full-bridges on primary H_A and secondary H_B side make the topology suitable for bidirectional operation. The transformer TR, with ratio $r = N_p/N_s$ between primary N_p and secondary N_s winding, compensates a high voltage difference between input voltage V_A and output voltage

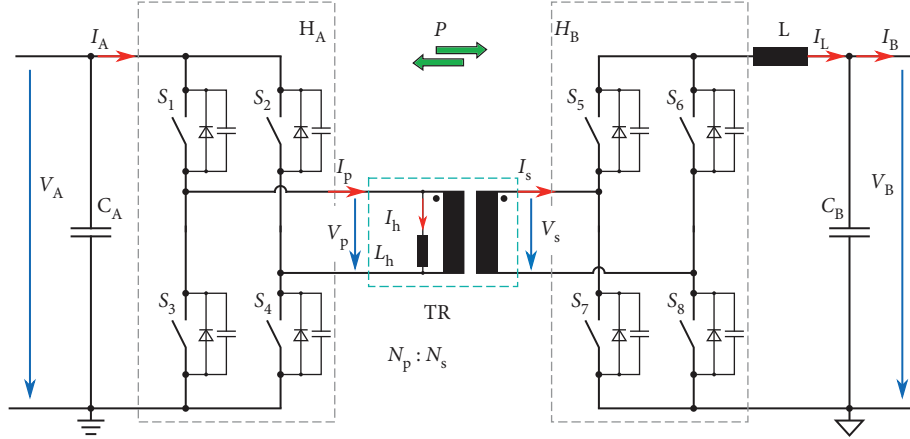


FIGURE 1: Phase-shift full-bridge converter topology. Two full-bridges H_A and H_B allow for bidirectional operation with power P . Transformer TR partially compensates high voltage difference between V_A and V_B and provides galvanic isolation.

$V_B = V_A/r d_{\text{eff}}$ to avoid low duty cycles d_{eff} with decreased efficiency. Additionally, its naturally galvanic isolation satisfies the normative requirements for e.g. battery chargers in electric vehicles for safety reasons [9]. Nevertheless, a transformer isolated converter suffers from issues such as an imbalance of magnetic flux resulting in an increasing DC-offset current $I_{h,DC}$ that drives the transformer into saturation [10]. To prevent damage due to high saturation currents and guarantee system reliability $I_{h,DC}$ must be eliminated.

Common topologies connect a blocking capacitor in series to the transformer in the main power path to suppress any DC-offset $I_{h,DC}$. However, placed in series with the transformer the blocking capacitor must be dimensioned for the maximum current of the converter at full power and additionally increases conduction losses due to its series resistance. As consequence the blocking capacitor is not preferred for applications with high power density and efficiency [11]. Considering bidirectional operation, a blocking capacitor must be placed in series to primary and secondary side of transformer. This method needs several additional power devices compared to controller-based methods and therefore results in increased size of power stage and overall system costs [12, 13].

Without additional passive devices in the main power path a controller needs to eliminate $I_{h,DC}$ [14]. Designing of a stable feedback control loop requires the measurement of $I_{h,DC}$ as process variable. However, considering the transformer as a four terminal device the acquisition of $I_{h,DC}$ is not directly possible as it overlays the transformer primary current I_p [15]. The current-mode control (CMC) is a very popular analog controller-based method to prevent the transformer from saturation. Its fast response due to analog comparators allows for stable operating conditions even at high switching frequencies f_{sw} . Unfortunately, in certain operating conditions instabilities, known as sub-harmonic oscillations, occur [16, 17]. The slope compensation technique normally is used to compensate the oscillation but overcompensation may result in a response delay [18, 19]. Additionally, the CMC method is not

suitable for flexible digital control schemes as it needs analog comparators [20].

Numerous research works concern the adjustment of PWM signals of power switches to balance the transformer magnetizing current in isolated DC-DC converters. However, the method of gathering the magnetizing current as process variable for a controller differs. [12] extends current-mode control with a hybrid peak and valley current control and does not need for slope compensation. The valley current detection requires AC-current sensing on the primary side of transformer with a suitable bandwidth for high switching frequencies. Considering bidirectional operation, the study in [21] uses primary and secondary transformer current to estimate magnetizing current from the previous switching period. A similar method in [22] only uses the averaged primary current to estimate the DC-offset from the previous period assuming the inductor current to be in steady state and average secondary current to be zero. [23] addresses the problem of magnetizing DC-offset causing DC-offsets in primary and secondary current. Here, two control loops need to scene also both, primary and secondary current and calculate the magnetizing current accordingly. In [24] a sensor directly measures the magnetic flux in the transformer core. The sensor requires modification of transformer core to mount the sensing coil through hole. An extended Kalman-Filter-approach to estimate the primary transformer current is presented in [25]. However, the study only concerns the discrimination of the transformer inrush current from internal faults to trigger a protective relay.

This article presents a novel digital feedback control loop scheme for eliminating DC-offset $I_{h,DC}$ without additional devices in the main power path. In contrast to related work a Luenberger observer is used that only requires the measurements of the transformer voltages to estimate the magnetizing current as process variable for a PI-controller. Main purpose of the study is to develop a digital controller that allows for simple application or flexible modification of existing controller structures only by adding the voltage measurement feature and to improve system reliability. At

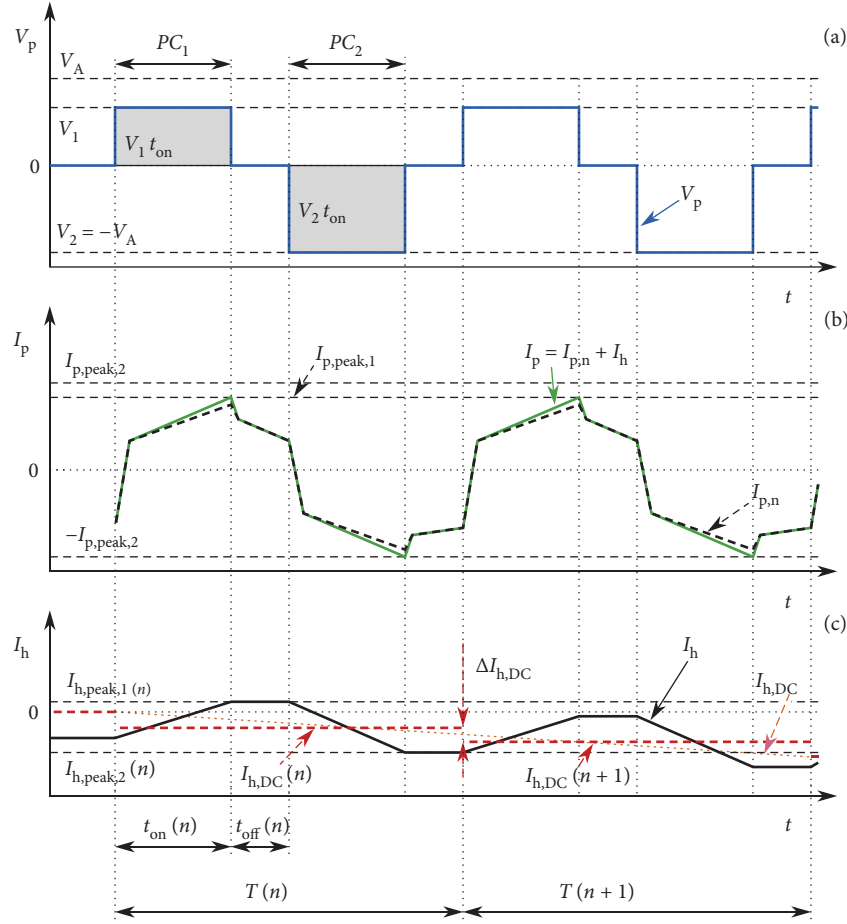


FIGURE 2: Schematic characteristics of transformer of PSFB with a present flux imbalance. (a) shows the applied primary voltage V_p . (b) explains the according primary current I_p as overlap between magnetizing current I_h and main primary side current $I_{p,n}$. (c) shows the course of magnetizing current I_h . The small asymmetrical voltage-second product in (a) causes a DC-offset $I_{h,DC}$ and its absolute value increases each period $T(n)$ till transformer saturation.

the beginning Section 2 explains the inevitable occurrence of DC-offset $I_{h,DC}$ in isolated PSFB converters in detail. In Section 3 conventional methods, like a blocking capacitor or CMC, used to overcome this problem are introduced. Section 4 explains the structure of the proposed digital control scheme. Section 5 describes an approach of acquiring the not measurable DC-offset $I_{h,DC}$ using a Luenberger observer with a detailed derivation of the state space model of the transformer and the subsequently design of the observer. In Section 6 the principal functionality of the proposed control scheme is evaluated by simulation and experimental results with an isolated PSFB converter prototype operating with a power $P = 1\text{kW}$ at a switching frequency $f_{sw} = 100\text{kHz}$. Finally, Section 7 gives a conclusion of the presented results.

2. Transformer DC-Offset Current

The magnetizing current I_h creates the magnetic field of the transformer required for power transfer from primary to secondary side and flows through the magnetizing inductor L_h of the transformer. I_h adds either to primary I_p or secondary current I_s of transformer depending on power

transfer direction. The transformer is not capable to transfer any DC component of I_h [26]. Therefore, the magnetizing current I_h needs to be detected on primary and secondary side when operating in bidirectional direction. The following considerations refer exemplary to a power transfer direction from primary side A with I_p to secondary side B with $I_s = (I_p - I_h)r$.

Figure 2 shows the typical schematic characteristics of applied voltage V_p in Figure 2(a), primary current I_p in Figure 2(b) and magnetization current I_h in Figure 2(c) for transformer of the PSFB converter shown in Figure 1.

The power transfer cycles PC_1 and PC_2 are determined according to the effective duty cycle $d_{eff} = 2t_{on}/T$ applied to the transformer TR. For desired duty cycle d_{eff} the phase-shift between lagging $S_1 + S_3$ and leading leg $S_2 + S_4$ of H_A varies and applies either the positive or the negative input voltage V_A to the magnetizing inductor L_h of the transformer TR according to Figure 2(a). For positive voltages $V_p > 0$ the magnetizing current I_h increases and for negative voltages $V_p < 0$, I_h decreases respectively. During the interval t_{off} no voltage is applied to L_h resulting in a constant I_h . The alternating positive and negative voltage-second products applied to the transformer within one period $T(n)$

determines the peak value $I_{h,\text{peak},1}$ and $I_{h,\text{peak},2}$, assuming to be constant during $T(n)$, in Figure 2(c) according to:

$$I_{h,\text{peak},1}(n) = \frac{1}{L_h} V_1 t_{\text{on}}(n) = \frac{1}{L_h} V_1 d_{\text{eff}}(n) \frac{T}{2}, \quad (1a)$$

$$I_{h,\text{peak},2}(n) = \frac{1}{L_h} V_2 t_{\text{on}}(n) = \frac{1}{L_h} V_2 d_{\text{eff}}(n) \frac{T}{2}. \quad (1b)$$

Therefore, the DC-offset $I_{h,\text{DC}}(n)$ can approximately be defined as the average value of magnetizing current $\bar{I}_h(n)$ during one period $T(n)$ with:

$$I_{h,\text{DC}}(n) = \bar{I}_h(n) = \frac{I_{h,\text{peak},1}(n) + I_{h,\text{peak},2}(n)}{2}. \quad (2)$$

Figure 2(b) explains the sloped magnetizing current I_h as an additional comparable small portion to the high main primary current $I_{p,n}$ with $I_h = I_p - I_{p,n}$ [15]. As consequence I_h cannot be measured directly considering the transformer as a four terminal device. Assuming negligible variations of $I_{p,n}$ and d_{eff} during one switching period $T(n)$ the DC-offset $I_{h,\text{DC}}(n)$ can be calculated from the difference between the peak values of I_p during one complete period $T(n)$ according to:

$$I_{h,\text{DC}}(n) = \frac{|I_{p,\text{peak},1}(n)| - |I_{p,\text{peak},2}(n)|}{2}. \quad (3)$$

For a present asymmetrical voltage-second product $V_1 \neq V_2$, the absolute value of $I_{h,\text{DC}}(n)$ increases each period $T(n)$ with

$$I_{h,\text{DC}}(n+1) = I_{h,\text{DC}}(n) + \Delta I_{h,\text{DC}} \quad (4)$$

and the resulting DC-offset $I_{h,\text{DC}} \neq 0$ drives the transformer into saturation. Ideally, the symmetrical structure of the PSFB topology ensures no DC-offset $I_{h,\text{DC}}$ as positive and negative current slope of I_h balance each other. Unfortunately, various inevitable effects can cause a small asymmetrical voltage-second product on primary side of transformer [14]. One transient reason is the unbalanced duty cycle between power cycle PC_1 for the lagging leg and PC_2 for the leading leg due to ZVS-operation or the change of d_{eff} for regulating the output current I_B of the PSFB [12]. Even in steady state operation manufacturing tolerances of devices as well as circuit board layout (PCB) cause different voltage drops and apply different voltages to the magnetizing inductor L_h and increase $I_{h,\text{DC}}$ [10]. Beside of the transformer the resulting high saturation current threatens the switching devices H_A and H_B and general system reliability. Additionally, the conduction loss unnecessarily increases with an unbalanced magnetizing current I_h as it does not contribute to power transfer from primary to secondary side. Therefore, system efficiency η is directly related to minimize $I_{h,\text{DC}}$.

3. Conventional Methods

Several methods have been proposed either to suppress or to control DC-offset $I_{h,\text{DC}}$ in [11, 12, 16, 17, 27, 28].

3.1. Blocking Capacitor. Connecting a blocking capacitor in series to the transformer suppresses any DC component in the transformer current I_p and allows for symmetrical operation [11]. Therefore, this method is suitable for acquiring only secondary side output current and apply proportional integral current control [27]. Additionally, in phase-shift control scheme the blocking capacitor method reduces the circulating currents during the free-wheel interval of the lagging leg and minimizes conduction loss. However, the timing of the leading leg becomes more complicated [12]. On the other hand, the blocking capacitor method simultaneously increases the conduction loss as the capacitor is located in the main power path with maximum current of the PSFB [28]. For bidirectional operation the magnetizing current I_h occurs on either side, primary and secondary, according to power direction. Therefore, this method needs two blocking capacitors and significantly increases volume and overall costs.

3.2. Current-Mode Control. The current-mode control (CMC) method is well known for non-isolated converters such as buck or boost converter topologies [16–18]. For non-isolated converters the inductor current I_L serves as process variable for the control loop. Fast response analog comparators generate PWM signals and directly trigger the power switches when inductor current I_L reaches a given threshold value and provide output control. Reference [18] distinguishes CMC between peak detect, valley detect and emulated control mode. However, either method suffers from sub-harmonic oscillation when inductor current I_L does not return to its initial value by the start of next switching cycle in continuous current-mode (CCM). In peak detect CMC the sub-harmonic oscillations occur at duty cycles $d_{\text{eff}} > 0.5$ and for valley detect at duty cycles $d_{\text{eff}} < 0.5$ respectively. A slope compensation circuit needs to correct the ripple current ΔI_L and results in a response delay for the controller [19]. In isolated converters the CMC method can additionally provide the elimination of DC-offset $I_{h,\text{DC}}$ with small modifications. Any DC component of I_h cannot pass the transformer. Therefore, the input current I_A must serve as process variable for $I_{h,\text{DC}}$ control with power direction from A to B side.

Figure 3 explains the compensation principle of CMC with the schematic characteristic curves of primary voltage V_p in Figure 3(a), input current I_A in Figure 3(b) and magnetizing current I_h in Figure 3(c) of transformer with a present flux imbalance. Neglecting parasitic inductors, the magnetizing current I_h slopes up with $m_1 = V_1/L_h$ during power cycle PC_1 and with $m_2 = V_2/L_h$ during power cycle PC_2 respectively. Parasitic effects reduce the applied voltage V_1 for power cycle PC_1 in Figure 3(a). Assuming a symmetrical duty cycle $d_1 = d_2 = d_{\text{eff}}$ for both power cycles the peak of input current $I_{A,\text{peak},1}$ does not reach the threshold value I_{th} of the analog comparator and the negative DC-offset $I_{h,\text{DC}} < 0$ rises [12]. The current-mode controller directly influences the duty cycle $d_{1,\text{CMC}} = 2t_{\text{on,CMC}}/T$ and extends $t_{\text{on,CMC}} > t_{\text{on}}$ until $I_{A,\text{peak},1}$ reaches the threshold current I_{th} . Therefore, the CMC ensures flux balance of the

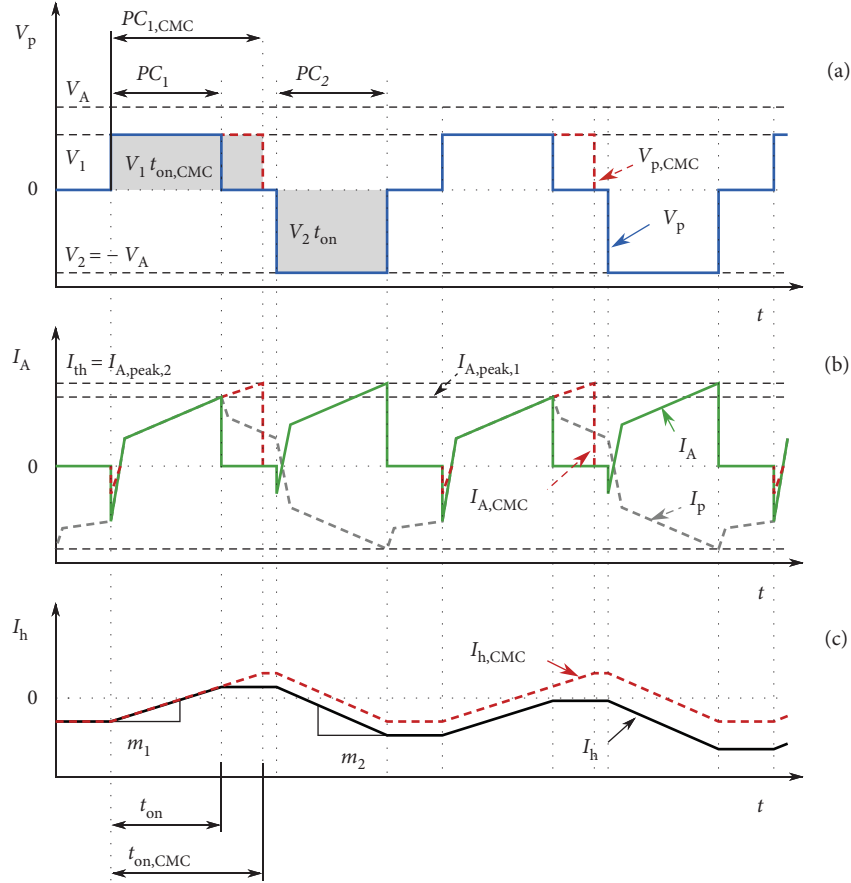


FIGURE 3: CMC compensation principle of PSFB with a present flux imbalance at transformer. (a) shows the primary voltage V_p , (b) the input current I_A and (c) the magnetizing current I_h of transformer as function of time. Reduced voltage $V_1 < V_2$ in power cycle PC_1 reduces $I_{A,peak,1}$ and results in an increasing negative DC-offset $I_{h,DC}$. CMC extends $t_{on,CMC}$ until $I_{A,peak,1}$ matches I_{th} with $I_{h,DC} = 0$ and provides a symmetrical voltage-second product.

transformer with $I_{h,DC} = 0$ and provides a symmetrical voltage-second product $V_1 t_{on,CMC} = V_2 t_{on}$ [12, 18].

Common control schemes prefer an analog controller with comparators compared to digital controller as the erratic increasing of I_A needs high bandwidth to detect the peak current $I_{A,peak}$ exactly. In consequence, the CMC is hard to combine with a flexible digital control scheme [20]. An additional challenge for the measured process variable I_A is the accuracy to properly detect the small portion of I_h as Figure 2(b) explains I_h as a comparable small additional sloped offset to the high input current I_A or rather $I_{p,n}$.

4. Proposed Control Scheme ctrIh

The proposed control scheme ctr_{Ih} uses flexible digital design. It requires neither lossy and expensive additional passive devices in the main power path of the PSFB nor analog comparator for triggering power switches. Similar to CMC, the proposed digital control scheme ctr_{Ih} directly interventions the duty cycle d_2 of the leading leg to equalize the peak values of primary current $|I_{p,peak,1}| = |I_{p,peak,2}|$ and eliminates any magnetizing DC-offset $I_{h,DC}$ within a few switching cycles.

Figure 4 depicts the control loop of the PSFB converter with ctr_{IL} for output current regulation and ctr_{Ih} for DC-offset $I_{h,DC}$ control. The output controller ctr_{IL} is built up with a PI-controller $PI_{IL}(z)$ and feedback control for the output voltage $V_B' = V_B + \Delta V_B$ for better adjustment of output operating point. The transfer function of the PSFB G_{duty} determines the effective duty cycle $d_{eff} = d_1 = V_B'/V_A r$ for desired output current $I_{B,set}$. The proposed magnetization controller ctr_{Ih} adds or subtracts a small offset Δd between duty cycle d_1 for the lagging and duty cycle $d_2 = d_1 + \Delta d$ for the leading leg until $I_{h,DC} = 0$. As $I_{p,n}$ and d_1 vary only a little during one switching period and also the impact of parasitic effects contribute only to a small amount, the ctr_{Ih} limits the magnitude of Δd to a few percentage of d_1 . Therefore, the influence of ctr_{Ih} on the output controller ctr_{IL} is negligible [14]. According to d_1 and d_2 the phase-shift calculator provides eight separate PWM signals for power switches S_1 – S_8 of PSFB power electronics. In the feedback path the main control unit (MCU) performs the acquisition of process variables V_A , V_B , I_L and I_h with analog digital converters (ADC). For output control the rippled inductor current I_L averages to the desired output current I_B . Therefore, the moving average finite impulse response (FIR)

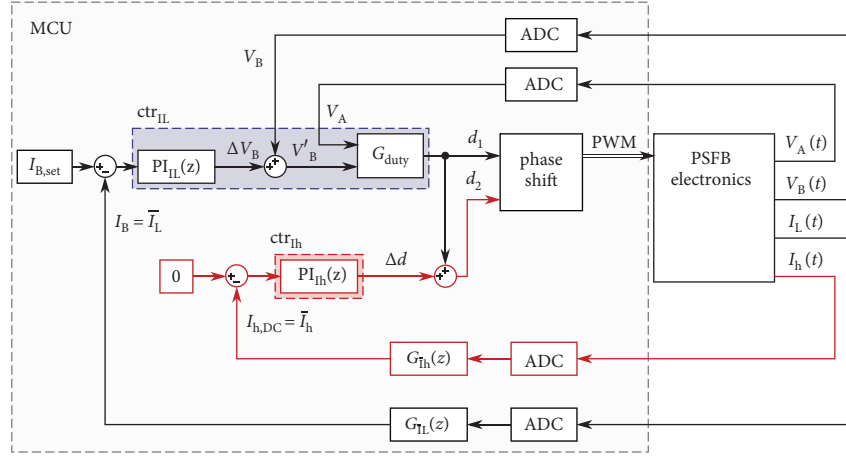


FIGURE 4: Control loop scheme of PSFB for $I_{h,DC}$ elimination. Output controller ctr_{IL} with $PI_{IL}(z)$ and G_{duty} determines duty cycle d_1 for desired $I_{B,set}$. The ctr_{Ih} adds a small offset Δd to d_1 of lagging leg until $I_{h,DC} = 0$. The phase-shift calculator translates the duty cycle information into eight phase shifted PWM signals for bidirectional operation of PSFB power electronics.

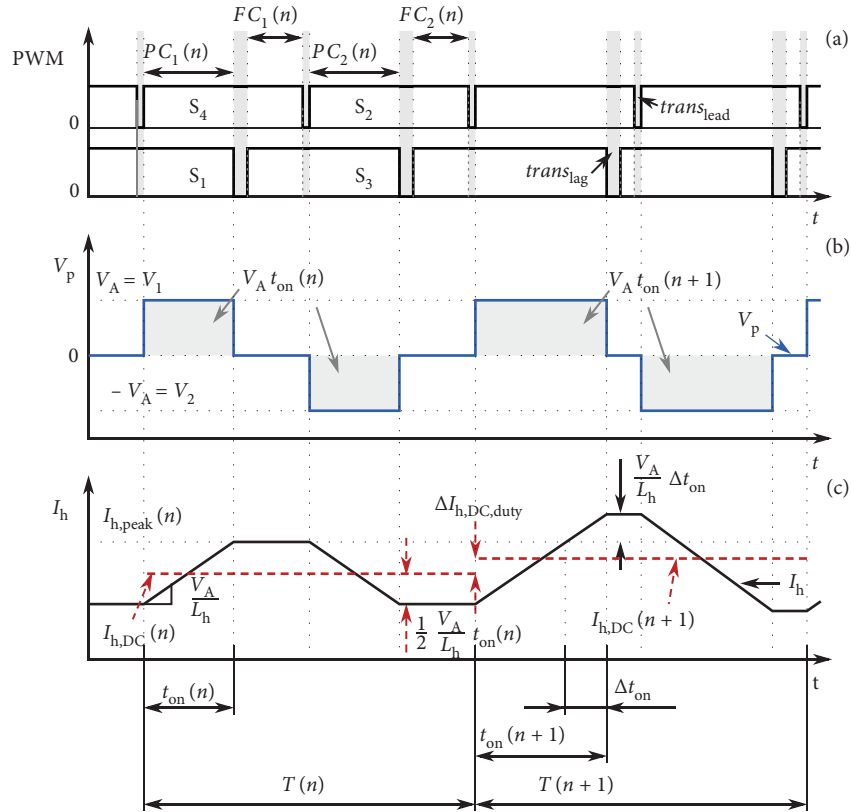


FIGURE 5: Influence of Δd on $\Delta I_{h,DC,duty}$ over two periods $T(n)$ and $T(n+1)$. According to phase shifted PWM signals for S_1 - S_4 in (a) the voltage V_p applies to transformer shown in (b). In (c) the different duty cycles $d_1(n+1) > d_1(n)$ cause a small difference $\Delta I_{h,DC,duty}$ between $I_{h,DC}(n+1)$ and $I_{h,DC}(n)$.

filter with $G_{IL}^- (z)$ averages I_L over N number of periods with:

$$I_B(n) = \frac{1}{N} \sum_{i=0}^{N-1} I_L(n-i). \quad (5)$$

Accordingly, the DC-offset $I_{h,DC}$ is defined as the average of rippled magnetization current I_h over several periods.

Again, a moving average FIR filter with $G_{Ih}^- (z)$ provides the process variable $I_{h,DC}$ of ctr_{Ih} . As V_A and V_B are already DC values there is no need for averaging with a FIR filter.

For proper design of ctr_{Ih} the relation $G_{Ih,DC}^- (z) = I_{h,DC}(z)/\Delta d(z)$ must be obtained. As mentioned before several effects, such as an unbalanced duty cycle either due to ZVS operation or output regulation as well as parasitic effects influence the occurrence of

unbalanced flux leading to $I_{h,DC} \neq 0$. Therefore, these effects have to be considered in the transfer function $G_{I_{h,DC}}(z)$. Figure 5 illustrates the influence of Δd on the DC-offset $\Delta I_{h,DC,duty}$ for analyzing the impact of unbalanced duty cycle due to output regulation ctr_{IL} over two consecutive switching periods $T(n)$ and $T(n+1)$. According to phase shifted PWM signals for power switches S_1 – S_4 in Figure 5(a) the voltage V_p in Figure 5(b) applies to the transformer. Figure 5(c) shows the time course of magnetizing current I_h resulting from unbalanced duty cycles $d_1(n) < d_1(n+1)$.

The PWM signals of power switches S_1 – S_4 obtain the duty cycle difference Δd to:

$$\Delta d = d_1(n+1) - d_1(n) = \frac{t_{on}(n+1) - t_{on}(n)}{T/2}. \quad (6)$$

Assuming equal voltages $V_1 = V_2 = V_A$ for power cycles $PC_1(n)$ and $PC_2(n)$ the magnetizing current I_h slopes with the same gradient $(V_1/L_h) = (V_2/L_h) = (V_A/L_h)$. In period $T(n+1)$, the output regulator ctr_{IL} increases $d_1(n+1) = d_1(n) + \Delta d$. Due to the increased duty cycle $d_1(n+1)$ the magnetizing current I_h surpasses the peak value $I_{h,peak}(n)$ before the end of power cycle $PC_1(n+1)$, thus, leading to an increased DC-offset in the following period $T(n+1)$ according to:

$$\Delta I_{h,DC,duty} = I_{h,DC}(n+1) - I_{h,DC}(n). \quad (7)$$

This behavior expresses also for small differences between duty cycle $d_1(n)$ and $d_2(n)$ in the same period $T(n)$.

Furthermore, $I_{h,DC}(n)$ defines as the average of magnetizing current $\bar{I}_h(n)$ with a linear slope V_A/L_h . Therefore, $\Delta I_{h,DC,duty}$ between two consecutive switching periods due to unbalanced duty cycle approximately calculates as follows:

$$\Delta I_{h,DC,duty} = \frac{1}{2} \left(\frac{V_A}{L_h} \Delta d \frac{T}{2} \right) = \frac{V_A T}{4L_h} \Delta d. \quad (8)$$

As long as there is a duty cycle imbalance Δd present, the magnetizing current $I_{h,DC}$ needs to diverge until the PSFB gets damaged if not compensated.

Another reason causing $I_{h,DC}$ are different parasitic resistances such as switch resistances or general PCB-design resulting in unequal voltages $V_1 \neq V_2$. [14] derives the influence of parasitic elements ΔR and can approximately be calculated as follows:

$$\Delta I_{h,DC,res} = \frac{\Delta RT}{2L_h} I_{h,DC}(n) = K_{res} I_{h,DC}(n). \quad (9)$$

As the impact of resistance is comparable low during transition times, (9) only considers the dominant time intervals of free-wheeling and power cycle. Regarding (9) parasitic resistances ΔR contribute proportionally with K_{res} to magnitude of $I_{h,DC}$. Therefore, the impact of $\Delta I_{h,DC,res}$ represents a steady-state fault of ctr_{Ih} [14].

During the transition between power PC_x and free-wheeling FC_x cycles mainly the switching characteristics of the power switches and dead time control influence the DC-offset $I_{h,DC}$. The dead time control determines different

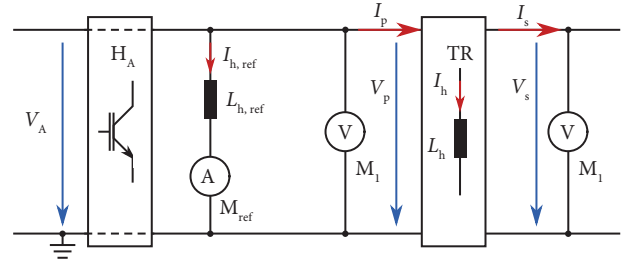


FIGURE 6: Simplified four terminal device of H_A and TR with voltage measuring method M_1 for estimating $I_{h,DC}$ with observer. Current measuring method M_{ref} serves as reference compared to conventional methods.

duty cycle d_1 for the lagging and d_2 for the leading leg according to ZVS-conditions. In [14], the detailed derivation results in:

$$\Delta I_{h,DC,trans} = K_{trans} I_{h,DC}(n). \quad (10)$$

again, with proportional gain K_{trans} .

For a unified transfer function $G_{I_{h,DC}}(z)$ the three main effects influencing $I_{h,DC}$ must be considered according to [14] with:

$$\Delta I_{h,DC} = \Delta I_{h,DC,duty} - \Delta I_{h,DC,res} - \Delta I_{h,DC,trans}. \quad (11)$$

The effects of resistance $\Delta I_{h,DC,res}$ and switch transition $\Delta I_{h,DC,trans}$ both prevent the development of $I_{h,DC}$ in either direction and therefore have to be subtracted while the transient $\Delta I_{h,DC,duty}$ supports the development of $I_{h,DC}$ [14].

Equation (12) calculates the transfer function of Δd and $I_{h,DC}$ in z domain as follows:

$$G_{I_{h,DC}}(z) = \frac{I_{h,DC}(z)}{\Delta d(z)} = \frac{V_A T}{4L_h} \frac{1}{z - K_{trans} - K_{res}}. \quad (12)$$

According to (12) the magnetization controller ctr_{Ih} requires an integrator for steady state stability. For the experimental results the ctr_{Ih} is implemented as PI-controller $PI_{Ih}(z)$.

5. Derivation of Observer Model

In the proposed digital control scheme of ctr_{Ih} , $I_{h,DC} = \bar{I}_h$ represents the process variable. Considering TR as a four terminal device with I_p and V_p as inputs and I_s and V_s as outputs, $I_{h,DC}$ cannot be measured at clamps directly. Therefore, $I_{h,DC}$ needs to be calculated from a related value depending on physically measurable in- and outputs.

In technical systems, a state observer is able to estimate an internal state value, such as $I_{h,DC}$ from measurable in- and outputs of the real system [29, 30]. Figure 6 simplifies a part of the PSFB converter with four terminal devices of full-bridge H_A and transformer TR . The measurable primary voltage V_p and secondary voltage V_s of transformer serve as in- and output for the observer model and allow for estimating the internal value of $I_{h,DC}$.

The state observer method is typically computer-implemented and therefore suitable for the proposed digital controller ctr_{Ih} .

The measuring method M_1 for the observer model requires only the average value of transformer voltages V_p and V_s and can be measured with operational amplifiers at naturally high bandwidth $BW > 1$ MHz. Additionally, the voltage measurement only needs small signal currents and therefore it is comparable lossless. The measuring method M_{ref} serves as reference to compare with conventional methods with an inductor $L_{h,\text{ref}}$ connected in parallel to transformer. According to:

$$I_h = \frac{L_{h,\text{ref}}}{L_h} I_{h,\text{ref}}, \quad (13)$$

the reference magnetization current $I_{h,\text{ref}}$ reflects the real magnetization current I_h and can be measured with a current clamp.

The proposed digital control scheme ctr_{Ih} uses the well-known Luenberger observer for estimation of $I_{h,\text{DC}}$ [30]. For the design of a Luenberger observer, in Section 5.1 first a stable linear state space model of the real transformer must be developed. Although the observer allows for controlling a time continuous system, a discretization is necessary for realistic applications with a digital control as described in Section 5.2. Section 5.3 examines the observability criteria according to Kalman of derived transformer model and Section 5.4 explains the design of the Luenberger gain parameters for observer model.

5.1. Transformer State Space Model. The Luenberger observer requires a linear state space model of transformer in form of:

$$\dot{x} = Ax + Bu, \quad (14a)$$

$$y = Cx + Du. \quad (14b)$$

In (14a) and (14b) x represents the state variables with input current i_p , output current i_s and magnetization current i_h . The primary voltage V_p represents the system input u and the secondary voltage V_s serves as measurable system output y according to:

$$x = [i_p \quad i_s \quad i_h]^T, \quad (15a)$$

$$u = V_p, \quad (15b)$$

$$y = V_s. \quad (15c)$$

Figure 7 shows the equivalent circuit diagram (ECD) of a real transformer. Parasitic resistances R_p and $R_{s,u}$ and leakage inductors L_p and $L_{s,u}$ depict the loss component of primary and secondary windings while R_{Fe} simulates the magnetic resistance of the transformer core. The core magnetization is regarded with magnetizing inductor L_h .

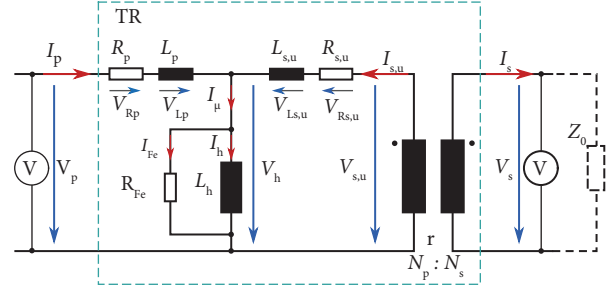


FIGURE 7: Equivalent circuit diagram of a real transformer TR regarding parasitic elements for loss and magnetization effects. Values with indexes s, u are referred to primary side with transformer ratio r .

Nonlinear behavior of magnetizing inductor L_h is neglected as the controller ctr_{Ih} prevents saturation of transformer. The ratio r of primary winding N_p to secondary winding N_s represents the ideal transformer TR with:

$$r = \frac{N_p}{N_s}. \quad (16)$$

In this model the parasitic capacitors are neglected as their time constants are very small compared to switching frequency and time constant of inductors. Z_0 represents the impedance of the load for gathering secondary current i_s .

The reference-arrow system in Figure 7 defines the sign of variables for further derivations. Secondary side values with indexes s, u are referred to primary side with respect to transformer ratio r according to:

$$V_{s,u} = rV_s, \quad i_{s,u} = -\frac{1}{r}i_s, \quad i'_{s,u} = \frac{1}{r}i_s, \quad R_{s,u} = (R_s + Z_0)r^2, \quad L_{s,u} = L_s r^2. \quad (17)$$

The Kirchhoff current (KCL) and voltage (KVL) laws obtain the main equations of the transformer model according to:

$$V_p = R_p i_p + L_p \dot{i}_p + L_h \dot{i}_h, \quad (18a)$$

$$V_s = -\frac{R_{s,u}}{r^2} i_s - \frac{L_{s,u}}{r^2} \dot{i}_s + \frac{L_h}{r} \dot{i}_h, \quad (18b)$$

$$V_s = -\frac{R_{s,u}}{r^2} i_s - \frac{L_{s,u}}{r^2} \dot{i}_s - \frac{L_p}{r} \dot{i}_p - \frac{R_p}{r} i_p + \frac{1}{r} V_p, \quad \text{with } V_s = Z_0 i_s, \quad (18c)$$

$$i_p = +\frac{1}{r} i_s + i_{Fe} + i_h, \quad \text{with } i_{Fe} = \frac{L_h}{R_{Fe}} \dot{i}_h. \quad (18d)$$

Reshaping (18a)–(18d) delivers the time continuous state space vector \dot{x} to:

TABLE 1: Transformer parameter for simulation and PSFB proto type.

Parameter	variable	value
Sampling time	t_s	2 [μ s]
Transformer ratio	r	2 [-]
Magnetization inductor	L_h	5000 [μ H]
Leakage inductor	L_p, L_s	6.23 [μ H]
Magnetic resistance	R_{Fe}	1000 [Ω]
Parasitic resistance (prim)	R_p	0.0045 [Ω]
Parasitic resistance (sec)	R_s	0.0070 [Ω]
Reference measuring inductor	$L_{h,ref}$	630 [μ H]

$$\dot{i}_p = +\frac{1}{L_p}V_p - \frac{R_{Fe} + R_p}{L_p}i_p + \frac{R_{Fe}}{L_p} \frac{1}{r}i_s + \frac{R_{Fe}}{L_p}i_h, \quad (19a)$$

$$\dot{i}_s = +\frac{R_{Fe}}{L_{s,u}}ri_p - \frac{R_{s,u} + R_{Fe}}{L_{s,u}}i_s - \frac{R_{Fe}}{L_{s,u}}ri_h, \quad (19b)$$

$$\dot{i}_h = +\frac{R_{Fe}}{L_h}i_p - \frac{R_{Fe}}{L_h} \frac{1}{r}i_s - \frac{R_{Fe}}{L_h}i_h. \quad (19c)$$

Referred to (14a) the system A and input B matrices can be obtained to:

$$A = \begin{bmatrix} \frac{R_{Fe} + R_p}{L_p} & \frac{R_{Fe}}{L_p} \frac{1}{r} & \frac{R_{Fe}}{L_p} \\ \frac{R_{Fe}}{L_{s,u}} r & -\frac{R_{s,u} + R_{Fe}}{L_{s,u}} & -\frac{R_{Fe}}{L_{s,u}} r \\ \frac{R_{Fe}}{L_h} & -\frac{R_{Fe}}{L_h} \frac{1}{r} & -\frac{R_{Fe}}{L_h} \end{bmatrix}, \quad (20a)$$

$$B = \begin{bmatrix} \frac{1}{L_p} & 0 & 0 \end{bmatrix}^T. \quad (20b)$$

The terms of voltage drop $(L_p/r)i_p$ and $(L_{s,u}/r^2)i_{s,u}$ in (18c) depend on the dynamic change of input and output current due to leakage inductors. However, the small time constant of transient process of leakage inductors in μ H-range is not detected due to FIR filtering of signal with G_{Th} . Neglecting the dynamic terms in (18c) provides the equation for system output V_s to:

$$V_s = \frac{1}{r}V_p - \frac{R_p}{r}i_p - \frac{R_{s,u}}{r^2}i_s. \quad (21)$$

with output matrix C and direct feed-through matrix D from (14b) according to:

$$C = \begin{bmatrix} \frac{R_p}{r} & -\frac{R_{s,u}}{r^2} & 0 \end{bmatrix}, \quad (22a)$$

$$D = \frac{1}{r}. \quad (22b)$$

TABLE 2: Poles of system matrix A for the three state variables i_p , i_s and i_h of transformer model.

state variable	poles
i_p	-6.4228×10^8
i_s	-2.0918×10^4
i_h	-3.1444

TABLE 3: Poles of reduced system matrix A_{red} for the two state variables i_s and i_h of transformer model.

state variable	poles
i_s	-2.0916×10^4
i_h	-2.4645

5.2. Analysis and Discretization of the Transformer Model. The transformer model includes three state variables i_p , i_s and i_h building a third order system with $\text{rank}(A) = 3$.

From the derived transformer model in the previous Section 5.1 the eigenvalues or poles of the system matrix A describe the dynamic behavior of the system.

The values in Table 1 refer to the measured values from PSFB prototype or from the corresponding data from manufacturer. Analyzing the system with transformer parameter according to Table 1 delivers the poles for all three state variables i_p , i_s and i_h shown in Table 2. As all poles are in the left-hand plane (LHP), the system provides stability [31].

The pole of i_p according to Table 2 is too fast for realistic sampling time $t_s = (T/5) = 2\mu$ s required for discretization of observer model. As the desired value of the observer only includes the state variable i_h , the state variable i_p with the fastest pole can be ignored. The reduction of system order eliminates the first state variable i_p and reconfigures the matrices A_{red} , B_{red} and C_{red} with $\text{rank}(A_{red}) = 2$ and poles according to Table 3.

Again, all poles of the system with reduced order are located in LHP with negative values. Therefore, also the reduced system is stable.

For realistic application of the observer, the reduced system matrices must be available in a discrete time form with sampling time t_s . The transfer of the reduced transformer model into discrete form affects only the system matrix A_{red} and the input matrix B_{red} [32]. One approach of discretization presented in [20] according to:

$$A_{d,red} = e^{A_{red}t_s}, \quad (23a)$$

$$A_{d,red} = \mathcal{L}^{-1}\{(sI - A_{red})^{-1}\}, \quad (23b)$$

delivers the discrete system matrix $A_{d,red}$ without approximation.

The MATLAB order of matrix exponential function $\exp m(A_{red}t_s)$ can directly perform the discretization and is suitable for the experimental approach.

With reduced discrete system matrix $A_{d,red}$ the reduced discrete input matrix $B_{d,red}$ calculates as follows:

TABLE 4: Poles of reduced discrete system matrix $A_{d,\text{red}}$ for the two state variables i_s and i_h of transformer model in Z -domain.

state variable	poles
i_s	0.9590
i_h	1.0000

$$B_{d,\text{red}} = \left(\int_0^{t_s} e^{A_{d,\text{red}} \tau} d\tau \right) B_{\text{red}}, \quad (24a)$$

$$B_{d,\text{red}} = A_{\text{red}}^{-1} (A_{d,\text{red}} - I) B_{\text{red}}. \quad (24b)$$

The reduced discrete output matrix $C_{d,\text{red}} = C_{\text{red}}$ and reduced discrete direct feed-through matrix $D_{d,\text{red}} = D_{\text{red}}$ are not affected and remain the same.

The analysis of the reduced discrete transformer model in Z -domain delivers the poles of $A_{d,\text{red}}$ according to Table 4 with one stable pole at $|z| < 1$ and one critically stable pole at $|z| = 1$. Therefore, a suitable design of the observer gain factors must guarantee the stability of the system.

5.3. Observability of the Transformer Model. To use the reduced discrete transformer model and realizing a Luenberger observer the reduced system must be observable. For a completely observable system the initial state $x(t=0) = x_0$ must be reconstructible from known input u and output value y within a finite time interval [31]. According to Kalman criteria of observability, the observability is proved if the observability matrix $S_{B d,\text{red}}$ in (25) has the same rank ($S_{B d,\text{red}}$) as the reduced system matrix $A_{d,\text{red}}$ with

$$S_{B d,\text{red}} = \begin{pmatrix} C_{d,\text{red}} \\ C_{d,\text{red}} A_{d,\text{red}} \end{pmatrix} = \begin{pmatrix} 94.2147 & 5.1102 \\ 90.3548 & 4.9009 \end{pmatrix}. \quad (25)$$

According to (25) the rank of observability matrix $\text{rank}(S_{B d,\text{red}}) = \text{rank}(A_{d,\text{red}}) = 2$ equals the rank of reduced discrete system matrix and so the system is completely observable. Additionally, its determinant $\det(S_{B d,\text{red}}) = -7.7102 \times 10^4 \neq 0$ is not zero [30, 33].

5.4. Design of Luenberger Observer. In the structure of a Luenberger observer the derived transformer model works in parallel to real transformer. The observer compares the measured output y with the calculated value of the transformer model \hat{y} and feeds back the estimation error $\Delta y_{\text{error}} = L(y - \hat{y})$ with feedback matrix L to the model [30].

From observer model the estimated state vector \hat{x} calculates as follows:

$$\dot{\hat{x}} = A_{d,\text{red}} \hat{x} + B_{d,\text{red}} u + \Delta y_{\text{error}}, \quad (26a)$$

$$\dot{\hat{x}} = A_{d,\text{red}} \hat{x} + B_{d,\text{red}} u + L(y - C_{d,\text{red}} \hat{x} - D_{d,\text{red}} u), \quad (26b)$$

$$\dot{\hat{x}} = (A_{d,\text{red}} - LC_{d,\text{red}}) \hat{x} + (B_{d,\text{red}} - LD_{d,\text{red}}) u + Ly. \quad (26c)$$

Suitable values of feedback matrix L adjust the dynamical behavior of the model to match the real transformer and

TABLE 5: Operating point for simulation and PSFB prototype at duty cycle $d_1 = 0.8$.

Parameter	variable	value
Input voltage	V_A	200 [V]
Input current	I_A	5.8 [A]
Output voltage	V_B	70 [V]
Charging current	I_B	14.1 [A]
Switching frequency	f_{sw}	100 [kHz]

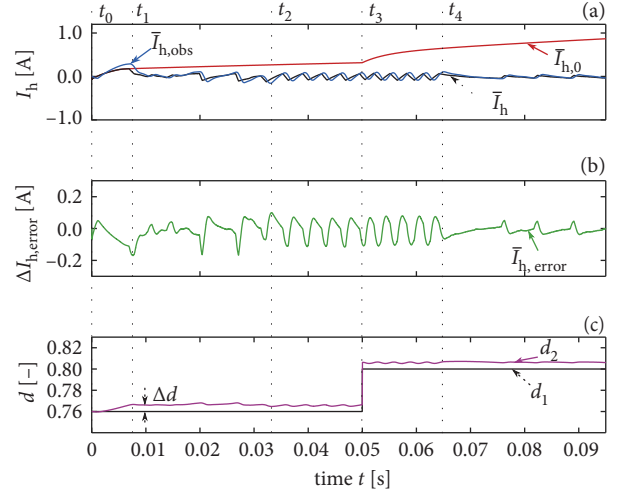


FIGURE 8: Evaluation of observer model. (a) shows the simulated average current \bar{I}_h and the estimated observer current $\bar{I}_{h,\text{obs}}$ compared to the uncontrolled current $\bar{I}_{h,0}$. (b) shows the model error $\Delta \bar{I}_{h,\text{error}}$ between \bar{I}_h and modeled $\bar{I}_{h,\text{obs}}$. (c) shows the influence of ctr_{Th} on controlled variable with d_1 and d_2 with offset $\Delta d \approx 0.07$.

react to disturbances or transient variations of duty cycle d_1 . The design of feedback matrix L with pole placement according to Ackermann [31, 33] is used and the known poles of $A_{d,\text{red}}$ from Table 4 deliver the first approach according to:

$$L = [0.00135 - 0.02478]^T. \quad (27)$$

6. Results

The proposed digital control scheme regulates the magnetizing current I_h of a PSFB to prevent transformer saturation. First approaches concern the simulation of electronics to prove principal functionality of ctr_{Th} , supported through experimental tests on a PSFB prototype with $P = 1\text{ kW}$. Table 5 lists the specifications of analyzed operating point of PSFB prototype electronics, also used for simulation.

To validate the simulated results in Section 6.1 the following Sections 6.2 and 6.3 explain the experimental measuring setup up and show the achieved results in operating point according to Table 5.

6.1. Simulation of Observer. For the evaluation of proposed ctr_{Th} in Section 4 and derived observer model in Section 5,

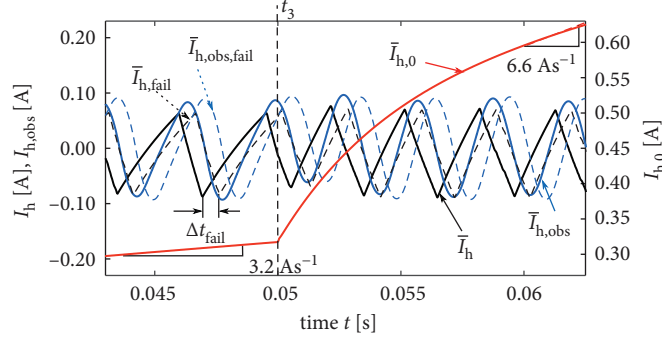


FIGURE 9: Behavior of magnetizing current in case of dynamic change of d_1 at t_3 . Uncontrolled $\bar{I}_{h,0}$ enlarges slope at t_3 with increased duty cycle d_1 and encourages transformer saturation. The controlled observer current $\bar{I}_{h,obs}$ matches the dynamic change and keeps \bar{I}_h around zero. $\bar{I}_{h,obs,fail}$ varies in phase due to model failure in $L_{h,fail}$.

the PSFB topology from Figure 1 is built up in a MATLAB/SIMSCAPE simulation model according to parameters in Table 1 and operating point listed in Table 5. The control scheme for ctr_{Ih} and observer model are implemented in MATLAB/SIMULINK.

The simulation results in Figure 8 demonstrate the behavior of the PSFB magnetizing current I_h at operating point in Table 5 for the different disturbances mentioned in Section 2, dynamic change of output current I_B through duty cycle d_1 and initial static differences due to manufacturing process of devices. Fluctuations of d_2 due to ctr_{Ih} thereby influence the magnetization current I_h in a similar way as d_1 . The simulation starts at t_0 with a desired output current $I_B = 9.3A$ and a corresponding duty cycle $d_1(t_0) = 0.76$. The series resistance $R_{S2} = R_{S1} + \Delta R = 0.2\Omega$ of switch S_2 is doubled compared to other switches with $R_{S1,3,4} = 0.1\Omega$, simulating an initial voltage-second product imbalance. Figure 8(a) shows the simulated average values for magnetizing current \bar{I}_h and estimated observer current $\bar{I}_{h,obs}$. Without ctr_{Ih} , the magnetizing current $\bar{I}_{h,0}$ steadily raises due to the unbalanced voltage-second product till saturation of transformer. In Figure 8(a) the observer current $\bar{I}_{h,obs}$ reflects the dynamic behavior of simulated current \bar{I}_h with the model error $\Delta\bar{I}_{h,error} = \bar{I}_h - \bar{I}_{h,obs}$ in Figure 8(b) fluctuating around zero with a DC-offset $\Delta\bar{I}_{h,error,DC} = 11mA$. The influence of ctr_{Ih} on controlled variable $\Delta d = |d_1 - d_2| \approx 0.07$ is shown in Figure 8(c).

The increased resistance R_{S2} forces ctr_{Ih} to increase $d_2 > d_1$ and compensates the voltage-second product imbalance. After initial transition process the ctr_{Ih} is able to correct the error resulting from static difference due to R_{S2} within $t_1 \approx 7.7ms$. Either change due to d_1 step at t_3 or d_2 control at t_2 and t_4 causes fluctuations in I_h . The estimated observer current $\bar{I}_{h,obs}$ follows the dynamics of \bar{I}_h with a small delay $\Delta t_{delay} = 0.5ms$ mainly resulting from computation and FIR filter. According to $\bar{I}_{h,obs}$ the ctr_{Ih} adjusts d_2 for regulating $I_{h,DC} = 0A$. Figure 9 explains the dynamic changes exemplary on d_1 in detail. At simulation time $t_3 = 50ms$ the desired output current raises to $I_B = 14.1A$ resulting in a dynamic change of duty cycle $d_1(t_3) = 0.8$. For $t < t_3$ the magnetizing current $\bar{I}_{h,0}$ approximately slopes up with $(d/dt)\bar{I}_h = 3.2As^{-1}$. For time $t_3 \leq t < t_3 + 50\mu s$ the

magnetizing current $\bar{I}_{h,0}$ steps up according to equation (8) and (9), raising $I_{h,DC}$. The step expresses as slope with $(d/dt)\bar{I}_{h,0} = 4.7mA(50\mu s^{-1})$ due to FIR filter G_{Fh} in MCU. With increased magnetizing current $\bar{I}_{h,0}$ the rising slope of magnetizing current $(d/dt)\bar{I}_h = 6.6As^{-1}$ due to R_{S2} enlarges after $t_3 + 50\mu s$ encouraging saturation of transformer. The controlled estimated observer current $\bar{I}_{h,obs}$ matches the dynamics of magnetizing current \bar{I}_h and the change can be controlled out by ctr_{Ih} with $I_{h,DC} \approx 0A$. According to applied to voltage V_p to L_h and moving average filter, the magnitude value results to $\bar{I}_{h,pp} \approx \bar{I}_{h,obs,pp} = 0.2A$.

For analyzing the resistance of ctr_{Ih} , $I_{h,obs,fail}$ exemplary represents the observer current with a model failure in magnetizing inductance $L_{h,fail} = 1.1L_h$. The model failure produces a time delay $\Delta t_{fail} = 1ms$ for $I_{h,fail}$ as the bigger magnetizing inductance reduces the slope of magnetizing current and enlarges the initial time t_1 for regulating the initial differences. Nevertheless, the ctr_{Ih} can handle the change in d_1 as well as in d_2 . A similar result is achieved with an examined model failure in primary resistance R_p and load impedance Z_0 .

6.2. Measurement Application. In the proposed control scheme the ctr_{Ih} only needs the average values of voltage V_p and V_s as measuring inputs to control the magnetization DC-offset $I_{h,DC}$. Typically, voltage measurements only need a network of low-cost resistors and operational amplifiers with naturally high bandwidth and low self-consumption. Therefore, voltage measurements reach higher efficiency than current measurements with high loss due to shunt resistors or hall sensors with limited bandwidth.

Figure 10 shows the measuring application for acquiring the input V_p and output V_s for the observer model. A simple voltage divider sets the transformer voltages to required $0 \dots 5V$ level of the main control unit MCU with $V_{p'}$ and $V_{s'}$. Depending on the switching state of full-bridge H_A the potential of the transformer voltage V_p is floating. As in single ended mode the MCU refers its input signals to GND_A , an operational amplifier $OP_{p'}$ performs the differential measurement $V_{p'} = V_{p'1} - V_{p'2}$ and provides stable and resilient signals for further processing in MCU.

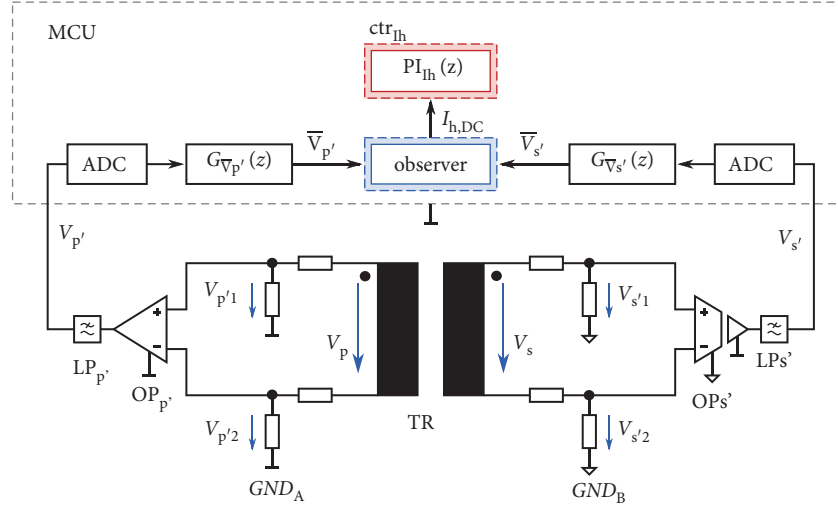


FIGURE 10: Measuring principle for in- and outputs of observer model. Voltage divider sets V_p and V_s to MCU voltage level. $OP_{p'}$ and $OP_{s'}$ perform differential measurement for $V_{p'}$ and $V_{s'}$ smoothed by $LP_{p'}$ and $LP_{s'}$. MCU averages values with $G_{\bar{V}_{p'}}(z)$ and $G_{\bar{V}_{s'}}(z)$ and estimates $I_{h,DC}$ according to observer model for ctr_{I_h} .

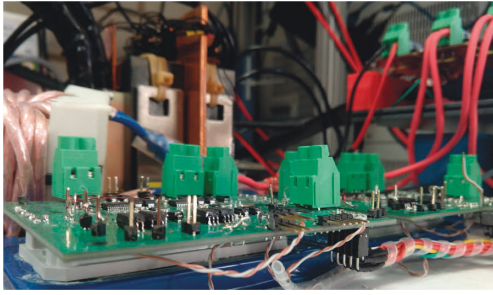


FIGURE 11: PSFB prototype used for experimental validation of proposed control scheme. The modular structure allows for flexible testing of different combination of power device.

Additionally, the differential measurement does not require a floating supply voltage V_{CC} for amplifiers. To maintain isolation of the PSFB the voltage measurement on secondary side $V_{s'}$ needs to be decoupled with an isolated amplifier $OP_{s'}$ after differential measurement.

The observer model only needs the average of voltage signals V_p and V_s . Therefore, the low pass filters $LP_{p'}$ and $LP_{s'}$ smooth the signals $V_{p'}$ and $V_{s'}$ and minimize the measuring noise due to rising edges with high dV/dt . In the MCU, the digital FIR filters $G_{\bar{V}_{p'}}(z)$ and $G_{\bar{V}_{s'}}(z)$ calculate the moving average over 1000 samples for averaging the signals. According to the observer model the MCU estimates $I_{h,DC}$ for ctr_{I_h} .

6.3. Experimental Results. Figure 11 shows the PSFB prototype used for the validation of the proposed control scheme. The modular structure splits the PSFB into 5 separate parts, full-bridges H_A and H_B in the front, transformer TR and filter inductor L in the back and a third circuit board equipped with the measuring devices and controller on the second floor to the right. Therefore, separate components can be substituted easily and allows for testing different

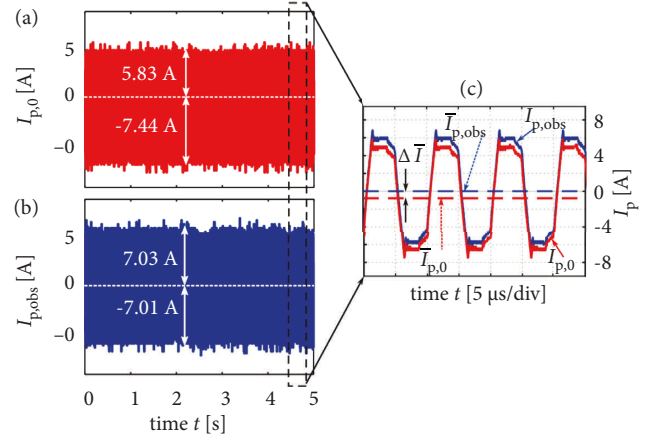


FIGURE 12: Experimental results of PSFB prototype in steady state operating point. (a) shows the primary current without ctr_{I_h} . The resulting asymmetrical course of $I_{p,0}$ leads to a negative offset $\bar{I}_{p,0} < 0$. In (b) ctr_{I_h} compensates the offset $\bar{I}_{p,obs} \approx 0$ and ensures a symmetrical course of magnetizing current. (c) explains the courses of primary currents in detail and illustrates the offset difference $\Delta \bar{I} = -806mA$.

power devices and combinations of the PSFB for optimization.

In the experimental test set up a National Instrument (NI) Data Acquisition (DAQ) system acquires the values from the measuring circuit board with $500MSs^{-1}$ and performs the calculations of the MCU. Therefore, the NI system includes the observer model, ctr_{I_h} control scheme with PI-controller and phase-shift calculator. The resulting eight PWM signals are generated on the counter outputs of NI system and directly connected to the drivers for full-bridge switches S_1 – S_8 .

For validating the observer model and simulation the effects of initial resistance differences and variable operating points are observed. Due to layout and manufacturing tolerances of devices, initial differences are not avoidable and

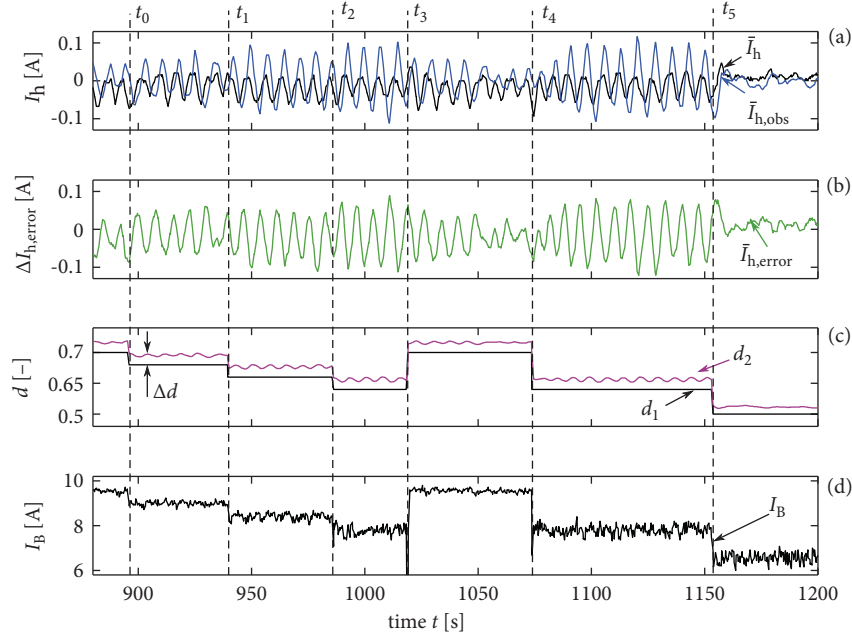


FIGURE 13: Experimental results of PSFB prototype in different operating points at times $t_0 - t_5$. (a) shows the averaged observer current $\bar{I}_{h,obs}$ following the dynamical behavior of real \bar{I}_h calculated from measurable reference current $\bar{I}_{h,ref}$. (b) illustrates the model error $\Delta\bar{I}_{h,error}$. In (c) ctr_{Ih} adjusts d_2 due to variation of d_1 and initial resistance differences. Changes of output current I_B due to d_1 are shown in (d).

present in prototype electronics. As the effect of resistance ΔR in real prototype is much smaller than in simulation, the rising slope of magnetizing current is smaller in experiment and allows for reacting before the prototype gets damaged.

First, Figure 12 compares the measured primary currents of the PSFB prototype in a steady state operating point according to Table 5. Figure 12(a) shows the primary current $I_{p,0}$ without any control of magnetization current while Figure 12(b) illustrates $I_{p,obs}$ controlled by ctr_{Ih} with observer model. Figure 12(c) explains the according courses of $I_{p,0}$ and $I_{p,obs}$ at higher temporal resolution.

The initial differences cause an unbalanced voltage-second product and lead to an asymmetrical course of $I_{p,0}$ with a negative average offset value of $\bar{I}_{p,0} = -848\text{mA}$. Without compensation this imbalance drives the transformer into saturation for continuous operating time. The ctr_{Ih} detects the initial imbalance and is able to regulate the average offset to a constant value of $\bar{I}_{p,obs} = -42\text{mA}$. Thus, the ctr_{Ih} removes the offset difference $\Delta\bar{I} = \bar{I}_{p,0} - \bar{I}_{p,obs} = -806\text{mA}$ and improves the system reliability and efficiency.

Figure 13 illustrates the results of the PSFB prototype controlled with ctr_{Ih} switching between different operating points. Therefore, during the experiment duty cycle d_1 varies each time $t_0 - t_5$ resulting in changed output current I_B shown in Figure 13(d).

In Figure 13(a) the magnetizing current $I_h = 0.126\bar{I}_{h,ref}$ is calculated from measurable reference current $\bar{I}_{h,ref}$ with parallel inductor $L_{h,ref}$ according to (13). Although the magnitude of observer current $I_{h,obs}$ is scaled due to feedback matrix L , the dynamical behavior reflects the magnetizing current \bar{I}_h and keeps the model error $\Delta\bar{I}_{h,error} = \bar{I}_h - \bar{I}_{h,obs}$ in Figure 13(b) around zero. Equal to theory and simulation in

Figure 13(c) the ctr_{Ih} adjusts d_2 with a constant offset $\Delta d = 0.1$ due to initial resistance differences and controls variations of d_1 . The exact measurement of the initial differences in the full-bridges of the prototype is very difficult and also vary due to temperature effects. Therefore, there is a difference between simulated duty offset $\Delta d = 0.07$ and prototype offset. However, the difference does not affect the functionality of the ctr_{Ih} . The magnetizing current in Figure 13(a) oscillates around its DC-offset $I_{h,DC} = -30\text{mA}$ while the ctr_{Ih} shows a better performance on $I_{h,obs,DC} = 1\text{mA}$. This difference results from measuring voltage offset due to operational amplifier and is the main drawback of the control scheme. Therefore, the measuring offset must be minimized by using offset compensated operational amplifiers. Compared to simulation the magnitude of magnetizing current is reduced. In real prototype there are also parasitic resistances in the PCB-Layout and in the supply lines from the source. As consequence the given input voltage V_A drops till the transformer with $V_p < V_A$ and decreases the slope of magnetizing current I_h . The magnitude of observer $I_{h,obs}$ and magnetizing current I_h vary each time $t_0 - t_5$ the operating point changes, as the controlling parameter for PI-controller $PI_{IL}(z)$ depend on I_B and were not modified during the experiment. Nevertheless, the effect on average values of \bar{I}_h or observer current $\bar{I}_{h,obs}$ is negligible and saturation can be prevented. Therefore, the experimental results confirm the results of simulation and prove the functionality of ctr_{Ih} for observed disturbances.

7. Conclusion

This paper presents a digital control scheme ctr_{Ih} for preventing saturation of the transformer due to flux

imbalances in isolated PSFB converters. As the magnetizing current I_h of a transformer, which is responsible for the saturation problem, cannot be measured directly, the proposed ctr_{Ih} uses a Luenberger observer for estimating the magnetizing current. Conventional methods overcome this problem either with increased costs and system size due to additional passive devices or need for lossy and bandwidth limited current measuring. As measuring inputs, the proposed ctr_{Ih} only needs the average values of transformer voltages V_p and V_s that can be measured with simple operational amplifiers with low self-consumption and naturally high bandwidth. The digital design of ctr_{Ih} allows for flexible implementation in the main control unit MCU of PSFB converters. Therefore, the MCU includes the ctr_{Ih} with Luenberger observer model and PI-controller, the output regulator ctr_{IL} as well as a phase-shift calculator and directly interventions the PWM signals for all power switches S_1 – S_8 via driver.

The paper identifies two inevitable effects as main reasons for increased magnetizing DC-offset current $I_{h,DC}$. First, initial resistance differences due to manufacturing tolerances of devices and second dynamic changes of duty cycle for regulating the output power. It is shown that without any control both effects would lead to transformer saturation and threaten system reliability. The proposed ctr_{Ih} with Luenberger observer model is evaluated by simulation and experimental results on a PSFB prototype with power $P = 1\text{kW}$ for the identified effects. The ctr_{Ih} is able to compensate initial resistance differences within 7.7ms by independently controlling the duty cycles of leading and lagging leg of the full-bridge. Also dynamic changes in duty cycle can be controlled out and guarantee a stable continuous operation with an magnetizing DC-offset $|I_{h,DC}| = 30\text{mA}$ at $V_A = 200\text{V}$. The differences between simulation and experiment can be explained through the additional voltage drop in the supply lines and PCB-layout that result in a smaller magnitude of I_h for the real prototype. The main drawback of the proposed scheme can be eliminated by using offset compensated operational amplifiers.

Data Availability

The datasets supporting the research are available from the corresponding author upon reasonable request.

Conflicts of Interest

The authors declare no conflicts of interest.

Acknowledgments

The authors would like to thank Hochschule Karlsruhe-University of Applied science and ads-tec Energy GmbH for facilitating this research.

References

- [1] <https://www.statista.com/statistics/222066/projected-global-energy-consumption-by-source/>.

- [2] J. Liu, W. Yao, J. Wen et al., "Impact of power grid strength and PLL parameters on stability of grid-connected DFIG wind farm," *IEEE Transactions on Sustainable Energy*, vol. 11, pp. 545–557, 2020.
- [3] A. Coester, M. W. Hofkes, and E. Papyrakis, "Economic analysis of batteries: impact on security of electricity supply and renewable energy expansion in Germany," *Applied Energy*, vol. 275, 2020.
- [4] P. Chatterjee and M. Hermwille, "Befeuern der DC-Ladeinfrastruktur-leistungsbausteine für schnelles Laden," *Emolility Tec Jan*, vol. 34–37, 2019.
- [5] J. M. Zhang, X. G. Xie, X. K. Wu, and Qian, "Zhaoming Comparison study of phase-shift full bridge ZVS converters," *IEEE 35th Annual Power Electronics Specialists Conference*, vol. 1, pp. 533–539, 2004.
- [6] Y.-Do Kim, K.-M. Cho, D. Y. Kim, and G. W. Moon, "Wide-range ZVS phase-shift full-bridge converter with reduced conduction loss caused by circulating current," *IEEE Transactions on Power Electronics*, vol. 28, no. 7, pp. 3308–3316, 2013.
- [7] H. Cha, L. Chen, R. Ding, Q. Tang, and Peng, "Fang zheng an alternative energy recovery clamp circuit for full-bridge PWM converters with wide ranges of input voltage," *IEEE Transactions on Power Electronics*, vol. 23, pp. 2828–2837, 2008.
- [8] J. A. Sabaté, V. Vlatkovic, R. B. Ridley, F.-C.- Lee, and B.-H.- Cho, *Design Considerations for High-Voltage High-Power Full-Bridge Zero-Voltage-Switched PWM Converter*, IEEE, Piscataway, NJ, USA, 1990.
- [9] Norm IEC 69/523/CD, *Electric Vehicle Conductive Charging System Part 23: DC Electric Vehicle Charging Station*, Beuth-Verlag, Berlin, Germany, 2017.
- [10] J. A. Claassens and I. W. Hofsjager, "A flux balancer for phase shift ZVS DC-DC converters under transient conditions," vol. 19, p. 5, Twenty-First Annual IEEE Applied Power Electronics Conference and Exposition (APEC), Phoenix, AZ, USA, 2006.
- [11] L. H. Mweene, C. A. Wright, and M. F. Schlecht, "A 1 kW 500 kHz front-end converter for a distributed power supply system," *IEEE Transactions on Power Electronics*, vol. 6, pp. 398–407, 1991.
- [12] J.-H. Ko, S.-W. Baek, K.-M. Lee, H.-W. Kim, K.-Y. Cho, and J.-M. Kim, "Hybrid current-mode control of PSFB converter to compensate slew interval and prevent magnetic saturation of transformers," *Electronics*, vol. 9, 2020.
- [13] T.-H. Kim, S.-J. Lee, and W. Choi, "Design and control of the phase shift full bridge converter for the on-board battery charger of the electric forklift," in *Proceedings of the 8th International Conference on Power Electronics-ECCE*, pp. 2709–2716, Asia, Jeju, Korea, 2011.
- [14] J.-H. Cho, K.-B. Park, J.-S. Park, G.-W. Moon, and M.-J. Youn, "Design of a digital offset compensator eliminating transformer magnetizing current offset of a phase-shift full-bridge converter," *IEEE Transactions on Power Electronics*, vol. 27, no. 1, pp. 331–341, 2012.
- [15] H. Schmidt-Walter and R. Kories, *Caption 2 Electric Field in Electrical Engineering-A Pocket Reference*, Springer-Verlag, Heidelberg, Germany, 2003.
- [16] F. Taeed and M. Nymand, "Adaptive slope compensation for high bandwidth digital current mode controller," in *IEEE 2015 IEEE 11th International Conference on Power Electronics and Drive Systems*, Piscataway, NJ, USA, 2012.
- [17] Y. Sun and B. Jiao, "Design of a soft-switched phase-shift full bridge converter," in *3rd International Conference on Systems and Informatics*, pp. 230–234, ICsAI, Shanghai, China, 2016.

- [18] R. Sheehan, *Understanding and Applying Current-Mode Control Theory*, National Semiconductor Corporation, Santa Clara, CA, USA, 2007.
- [19] N. Kondrath and M. K. Kazimierczuk, "Slope compensation and relative stability of peak current-mode controlled PWM dc-dc converters in CCM," in *IEEE 56th International Midwest Symposium on Circuits and Systems*, pp. 477–480, MWSCAS), Columbus, OH, USA, 2013.
- [20] J. Chen, A. Prodic, R. W. Erickson, and D. Maksimovic, "Predictive digital current programmed control," *IEEE Transactions on Power Electronics*, vol. 18, no. 1, pp. 411–419, 2003.
- [21] Y. Panov, M. M. Jovanovic, and B. T. Irving, "Novel transformer-flux-balancing control of dual-active-bridge bidirectional converters 2015," *IEEE Applied Power Electronics Conference and Exposition (APEC)*, 2015.
- [22] K. H. Andersen and M. Nyman, "Fast Digital estimating and balancing of transformer magnetizing current in an isolated full bridge converter 2017," *IEEE Southern Power Electronics Conference (SPEC)*, vol. 1–6, 2017.
- [23] Y. Panov, M. M. Jovanovic, L. Gang, and M. Yueyong, "Transformer-flux-balancing control in isolated bidirectional DC-DC converters 2014," *IEEE Applied Power Electronics Conference and Exposition-APEC*, pp. 49–56, 2014.
- [24] K. Umetani, Y. Itoh, and M. Yamamoto, "Adetection method of dc magnetization utilizing local inhomogeneity of flux distribution in power transformer core," pp. 3739–3746, IEEE Energy Conversion Congress and Exposition (ECCE), Piscataway, NJ, USA, 2014.
- [25] F. Naseri, Z. Kazemi, M. M. Arefi, and E. Farjah, "Fast discrimination of transformer magnetizing current from internal faults: an extended kalman filter-based approach," *IEEE Transactions on Power Delivery*, vol. 33, no. 1, pp. 110–118, 2018.
- [26] M. Schühle, M. Beltle, S. Tenbohlen, and BonmannD, "Development of a simulation model to inspect magnetic flux in power transformer components in case of saturation," *VDE-Hochspannungstechnik*, vol. 14, 2016.
- [27] N. Kutkut and G. Luckjiff, "Current mode control of a full bridge DC-to-DC converter with a two inductor rectifiers," in *Proceedings of the 28th Annual IEEE Power Electronics Specialists Conference. Formerly Power Conditioning Specialists Conference 1970-71. Power Processing and Electronic Specialists Conference 1972 (PESC97)*, pp. 203–209, St. Louis, MO, USA, 1997.
- [28] J.-G. Cho, J. A. Sabate, G. Hua, and F. C. Lee, "Zero-voltage and zero-current-switching full bridge PWM converter for high-power applications," *IEEE Transactions on Power Electronics*, vol. 11, no. 4, pp. 622–628, 1996.
- [29] R. G. Raj, S. Palani, and H. H. Sait, "State space modeling and implementation of a new transformer based multilevel inverter topology with reduced switch count," *Circuits and Systems*, vol. 07, no. 04, pp. 446–463, 2016.
- [30] J. Lunze, *Regelungstechnik 2: MehrgröSSensysteme Digitale Regelung* Springer-Verlag, Heidelberg, Germany, 2008.
- [31] O. Föllinger, *Regelungstechnik, Einführung in die Methoden und ihre Anwendung* Hüthig Verlag, Heidelberg, Germany, 1994.
- [32] C.-T. Chen, *State-Space Solutions and Realizations in Linear System Theory and Design*, pp. 90–96, Oxford University Press, Oxford, US, 1993.
- [33] J. Ackermann, *Der Entwurf linearer Regelungssysteme im Zustandsraum*, pp. 90–96, M.I.T. Press, Cambridge, MA, USA, 1972.